Magazine of Concrete Research, 2010, **62**, No. 1, January, 25–38
doi: 10.1680/macr.2008.62.1.25

Behaviour of a hollow RC column with an internal tube

T. H. Han*, J. M. Stallings†, S. K. Cho‡ and Y. J. Kang§

Seoul Metro; Auburn University; Seoul National University of Technology; Korea University

A non-linear column model of an internally confined hollow (ICH) reinforced concrete (RC) column was suggested and column tests were performed. The suggested column model considered the confining effect and the material non-linearity of the concrete. To verify the suggested column model and to investigate the behaviour of an ICH RC column, quasi-static tests were performed for three different ICH RC columns and a solid RC column. The analysis results by the suggested model were agreeable with the test results, and they showed that it was reasonable to consider the confining effect of concrete. The test results showed that an ICH RC column has high strength, high energy-absorbing capacity, a normal damage index and acceptable ductility, which can be controlled by the thickness and the type of its internal tube.

Notation

A_{sp}	cross-sectional area of a transverse reinforcement
D'	diameter of confined core concrete (from the centre of a transverse reinforcement to the centre of its opposite side)
DI	damage index
D_i	diameter of hollow section
d_{bl}	diameter of the longitudinal reinforcement
dE_n	absorbed energy of the column per cycle
d_m	maximum displacement of the column per cycle
d_u	ultimate displacement of the column
E_c	tangent modulus of unconfined concrete
e_b	balanced eccentricity
$F_{L,j}$	lateral force at the jth stage of the strain distribution
f_{bk}	buckling strength or snap-through buckling strength of the internal tube
f_c	stress acting on concrete
f'_c	strength of unconfined concrete
f'_{cc}	confined strength of concrete
f_l	confining pressure
f'_l	effective constant lateral confining pressure
f'_{lc}	effective constant lateral confining pressure in the circumferential direction
f_{lim}	smaller value between yield strength and buckling strength of the internal tube
f_{lc}	confining stress in the circumferential direction
f_{lr}	confining stress in the radial direction
f_{tube}	stress acting on the internal tube
f_u	ultimate strength of the steel tube or the reinforcement
f_y	yield strength of the steel tube or the reinforcement
f_{ye}	yield strength of the longitudinal reinforcement
f_{yh}	yield strength of a transverse reinforcement
f_{yt}	yield strength of the internal tube
k_e	reduction coefficient for the effective constant lateral confining pressure
L	height of the column
L_H	distance from the critical section of the plastic hinge to the point of contraflexure
L_p	length of the equivalent plastic hinge
M_0	nominal moment without axial load
M_b	nominal moment under balanced condition
M_j	moment at the jth stage of the strain distribution
M_j^{CC}	moment acting on core concrete at the jth stage of the strain distribution
M_j^{CV}	moment acting on cover concrete, at the jth stage of the strain distribution

* R&D Center, Seoul Metro, Seoul, 137-060, Korea
† Department of Civil Engineering, Auburn University, Auburn, Alabama, 36830, USA
‡ School of Civil Engineering, Seoul National University of Technology, Seoul, 139-743, Korea
§ Department of Architectural, Civil and Environmental Engineering, Korea University, Seoul, 156-701, Korea

(MACR 800171) Paper received 8 October 2008; last revised 18 March 2009; accepted 11 May 2009

www.concrete-research.com 1751-763X (Online) 0024-9831 (Print)

M_j^{R} moment acting on longitudinal reinforcements at the jth stage of the strain distribution
M_j^{T} moment acting on the internal tube at the jth stage of the strain distribution
M_{n} nominal moment capacity of the column
M_{u} maximum moment capacity of the column
P_0 nominal axial strength without eccentricity
P_{b} nominal axial strength under balanced condition
P_j axial load at the jth stage of the strain distribution
P_j^{CC} axial load acting on core concrete at the jth stage of the strain distribution
P_j^{CV} axial load acting on cover concrete at the jth stage of the strain distribution
P_j^{R} axial load acting on longitudinal reinforcements at the jth stage of the strain distribution
P_j^{T} axial load acting on internal tube at the jth stage of the strain distribution
Q_{y} yield strength of the column under static state
t thickness of the internal tube
t_{bk} required minimal thickness of the internal tube to avoid its buckling failure
t_{eq} equivalent thickness of the corrugated internal tube
t_{yt} required minimal thickness of the internal tube to avoid its yielding failure
β reduction factor.
Δ_{p} plastic displacement of the column
Δ_{y} yield displacement of the column
ε axial strain of concrete
$\varepsilon_{\mathrm{cc}}$ axial strain of concrete at its peak strength
$\varepsilon_{\mathrm{co}}$ axial strain of unconfined concrete at its peak strength
$\varepsilon_{\mathrm{cu}}$ ultimate strain of the concrete
ε_{u} ultimate strain of the steel tube or the reinforcement
ε_{y} yield strain of the steel tube or the reinforcement
θ_{p} plastic rotation of the column
φ_j curvature of the column at the jth stage of the strain distribution
ϕ_{p} plastic curvature capacity
ϕ_{u} ultimate curvature corresponding to the ultimate strain of the concrete
ϕ_{y} yield curvature

Introduction

A hollow reinforced concrete (RC) column has been popularly used for more economic design by reducing its material and self-weight. It has high effectiveness of section properties but it may show a brittle failure at its inner face. This brittle failure results from the absence of the confinement at the inner face, whereas the outer core concrete is appropriately confined by transverse reinforcements. The existence of the hollow section makes the concrete confined biaxially, although it is confined by transverse reinforcements. The strength of the hollow RC column can be enhanced if its concrete is confined triaxially. Based on this idea, Kim *et al.* (2001) suggested a hollow RC column with a steel tube. Han *et al.* (2008) proposed a non-linear concrete model for an internally confined hollow (ICH) RC column based on Mander *et al.*'s (1984) unified concrete model. Figure 1 shows the cross-section of an ICH RC column.

Because confined concrete shows enhanced strength and ductility compared with unconfined concrete, many researchers have studied the confinement and its effects on concrete. Roy and Sozen (1964) tested rectangular RC concrete members confined by transverse reinforcements. They stated that there was no increase in concrete strength, but a significant increase in ductility could be achieved. Iyengar *et al.* (1970) and Desayi *et al.* (1978) showed that there was a significant increase in both strength and ductility of concrete members including circular steel spirals. Some other researchers (Scott *et al.*, 1982; Sheikh and Uzumeri, 1980; Vallenas *et al.*, 1977) tested realistically scaled specimens of building columns, and they presented the stress–strain relationships of the RC column. The test results of confined square sections with rectangular- and octagonal-shaped transverse reinforcements indicated that the strength and the ductility of the specimens were significantly enhanced. Recently, many researchers (Chung *et al.*, 2002; Fafitis and Shah, 1985; Sakino and Sun, 1984; Sheikh and Uzumeri, 1982) have made analytical models for the explanation of the effect of concrete confinement. The analytical results showed widely divergent opinions about the increase in strength and ductility of confined concrete as the shape of the confined section. Mander *et al.* (1984) suggested a unified concrete model to define the stress–strain relations for square and circular sections; this is widely used to explain the effect of concrete confinement.

These researches focused on confining the outside of an RC column. They are effective in confining a solid RC column triaxially. However, they are not so effective in confining a hollow RC column because its concrete is confined biaxially. Therefore, to confine the concrete in a hollow RC column triaxially, it is necessary to confine the concrete of the inner face of the column. To confine the concrete of a hollow RC column triaxially, an ICH RC column was introduced by Kim *et al.* (2001) and its non-linear concrete model was proposed by Han *et al.* (2008). An ICH RC column is a hollow RC column having a flat or corrugated tube inside itself to confine the concrete internally. In this study, a non-linear column model for an ICH RC column was suggested by using Han *et al.*'s (2008) concrete model and column tests were performed to investigate the behaviour of the ICH RC column. Three different ICH RC columns and one solid RC column were tested.

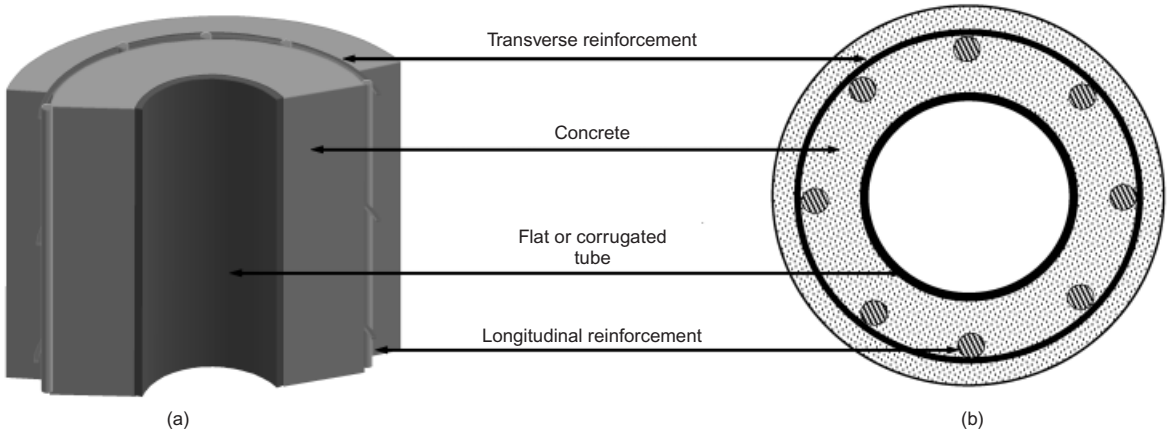

Figure 1. Cross-section of a circular ICH RC column

Analytical model

Concrete model

Failure mode of ICH RC column. Han *et al.* (2008) proposed a concrete model for an ICH RC column, and they defined the failure modes of an ICH RC column. To define the failure mode, the confining condition was determined if the concrete was under biaxial or triaxial confinement. Figure 2 shows a free body diagram for the half section of an ICH RC column when axial load acts on the concrete only. Considering the failures of the internal tube and the transverse reinforcement, three failure modes can be defined as Equation 1. In the first failure mode, the internal tube fails by buckling or yielding before the transverse reinforcement yields. The reverse condition is the second failure mode. In the third failure mode, the internal tube and transverse reinforcement fail simultaneously.

$$f_{tube} > f_{lim} = \text{smaller } (f_{yt}, f_{bk}): \text{ failure mode 1} \quad (1a)$$

$$f_{tube} < f_{lim} = \text{smaller } (f_{yt}, f_{bk}): \text{ failure mode 2} \quad (1b)$$

$$f_{tube} = f_{lim} = \text{smaller } (f_{yt}, f_{bk}): \text{ failure mode 3} \quad (1c)$$

Equilibrium in ICH RC column. In the first failure mode, the concrete in an ICH RC column is triaxially confined until the internal tube fails. After the internal tube fails, it is assumed to exert no more passive confining pressure by the internal tube. Therefore, after the internal tube fails, the concrete in the column is under biaxial confinement. In the second failure mode, the concrete in the column is triaxially confined until the column fails by the yielding of the transverse reinforcement. The failure of the whole column member depends on the yielding of the transverse reinforcement. The third failure mode shows a failure pattern similar to the second failure mode. Before the failure of the internal tube, the confining pressure can be derived as Equation 2 from Figure 2(a). From Figure 2(b), the stress acting on the internal tube is derived as Equation 3. Therefore, the derived confining pressure is equal to that of a solid RC column. After the internal tube fails, the concrete is confined biaxially, and it is the same condition as a hollow RC column ($f_{lc} \neq f_{lr} = 0$). In this case, the confining pressure in the circumferential direction is derived as Equation 4 from Figure 2(a), assuming that f_{lr} is zero

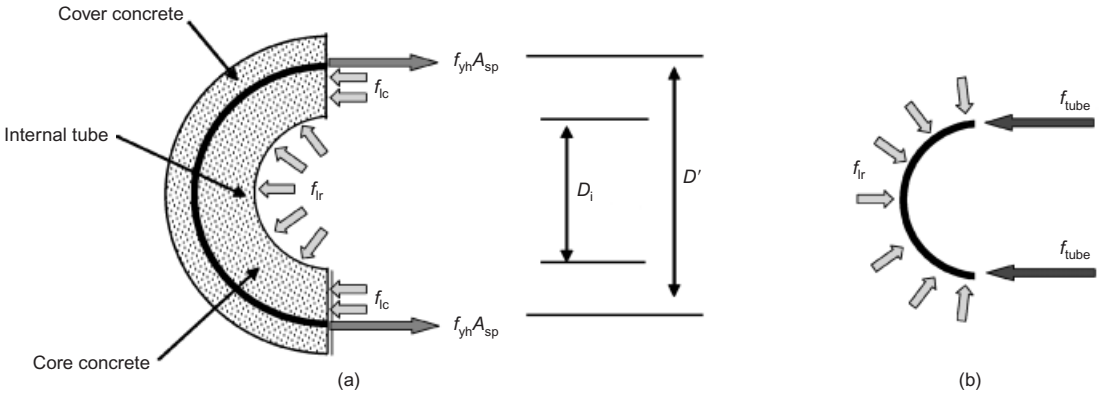

Figure 2. Confining stress on concrete in an ICH RC column: (a) FBD for concrete and reinforcement; (b) FBD for internal tube

$$f_l = \frac{2f_{yh}A_{sp}}{D's} \quad (2)$$

$$f_{tube} = \frac{f_l D_i}{2t} \quad (3)$$

$$f_{lc} = \frac{2f_{yh}A_{sp}}{(D' - D_i)s} \quad (4)$$

Because the yield strength and the buckling strength of a steel tube depend mainly on the thickness of the tube, the failure mode can be controlled by the thickness of the internal tube. Considering the yielding condition of the internal tube, Equation 5 is given from Equation 2 and Equation 3. To induce the failure of the transverse reinforcement before the internal tube yields, the stress acting on the internal tube must be smaller than f_{yt}. By the stress requirement of the internal tube of Equation 5, the thickness requirement can be derived as Equation 6. If the internal tube satisfies Equation 6, it does not yield before the transverse reinforcement yields

$$f_{tube} = \frac{D_i f_{yh}A_{sp}}{D'st} < f_{yt} \quad (5)$$

$$t > \frac{D_i f_{yh}A_{sp}}{D'sf_{yt}} = t_{yt} \quad (6)$$

Because the internal tube of an ICH RC column is unilaterally restrained by concrete, it has different buckling strength from that of an arch or a ring with bilateral boundary conditions. Han *et al.* (2008) assumed that the buckling behaviour of the internal tube could be considered as the snap-through behaviour of a circular shallow arch because their buckled shapes were similar to each other. They adopted the buckling coefficient proposed by Kerr and Soifer (1969) to estimate the buckling strength of the internal tube. Therefore, the snap-through buckling strength of the internal tube can be calculated with Equation 7

$$f_{bk} = \frac{2{\cdot}27}{3}\frac{t^2E}{D_i^2} \quad (7)$$

To prevent the premature buckling failure of the internal tube before a transverse reinforcement yields, the buckling strength of the internal tube must be larger than the confining pressure acting on concrete when the transverse reinforcement yields. Therefore, a failure criterion can be defined as Equation 8. From Equation 8, t_{bk} can be derived as Equation 9. When a corrugated tube is used as the internal tube, the equivalent thickness of the internal tube is calculated with Equation 10 by utilising Timoshenko and Woinowsky-Krieger's (1959) research.

$$f_{bk} = \frac{2{\cdot}27}{3}\frac{t^2E}{D_i^2} > f_l = \frac{2f_{yh}A_{sp}}{D's} \quad (8)$$

$$t > \sqrt{\frac{6}{2{\cdot}27}\frac{D_i^2 f_{yh}A_{sp}}{D'Es}} = t_{bk} \quad (9)$$

$$t_{eq} = \sqrt[3]{6f^2t\left[1 - \frac{0{\cdot}81}{1 + 2{\cdot}5\left(\frac{f}{2l}\right)^2}\right]} \quad (10)$$

Stress–strain relation. Han *et al.*'s (2008) concrete model is based on the unified concrete model proposed by Mander *et al.* (1984). Mander *et al.* (1984) adopted Equation 11 proposed by Popovics (1973) to develop the unified stress–strain relation of the confined concrete. This model is based on a constant confining pressure.

$$f_c = \frac{f'_{cc}xr}{r - 1 + x^r} \quad (11a)$$

$$x = \frac{\varepsilon}{\varepsilon_{cc}} \quad (11b)$$

$$r = \frac{E_c}{(E_c - E_{sec})} \quad (11c)$$

$$E_{sec} = \frac{f'_{cc}}{\varepsilon_{cc}} \quad (11d)$$

For the triaxially confined concrete, the peak concrete strength is calculated with Equation 12. For the biaxially confined concrete, the peak concrete strength is calculated with Equation 13 (Han *et al.*, 2008). The strain at peak concrete strength is calculated with Equation 14.

$$f'_{cc} = f'_c\left(2{\cdot}254\sqrt{1 + \frac{7{\cdot}94f'_l}{f'_c}} - \frac{2f'_l}{f'_c} - 1{\cdot}254\right) \quad (12)$$

$$f'_{cc} = -2{\cdot}75\frac{f'^2_{lc}}{f'_c} + 1{\cdot}835f'_{lc} + f'_c \quad (13)$$

$$\varepsilon_{cc} = \varepsilon_{co}\left[1 + 5\left(\frac{f'_{cc}}{f'_c} - 1\right)\right] \quad (14)$$

In an RC column, transverse reinforcements cannot confine the entire core concrete completely. Therefore, f_l should be replaced by f'_l. The effective constant confining pressure can be calculated by Equation 15 using k_e

$$f'_l = k_e f_l \quad (15)$$

Column model

To predict the behaviour of an ICH RC column, a column analysis model was suggested in this study based on Han *et al.*'s (2008) concrete model. This analysis tool is capable of axial load–bending moment interaction analyses and lateral load–lateral displacement analyses. It uses section analysis, accounting for equilibrium, strain compatibility, material stress–strain curves and adopted the layer-by-layer technique for numerical integration of stresses (Kilpatrick and Ranagan, 1997). The analyses are conducted for two conditions including (a) unconfined concrete stress–strain curve and elasto-plastic steel behaviour and (b) con-

fined concrete stress–strain curve and accounting for strain hardening of the steel. Figure 3 shows the idealised section. Figure 4 shows the adopted stress–strain curves. The analyses are performed as the stage of strain distribution as shown in Figure 5. For the each stage of strain distribution, stresses acting on the concrete, the longitudinal reinforcements and the internal tube are calculated. By summation of them, the axial load and the moment are calculated for each stage of the strain distribution. P_j, M_j and ϕ_j are given by Equation 16, Equation 17 and Equation 18 respectively.

$$P_j = P_j^{CC} + P_j^{CV} + P_j^{R} + P_j^{T} \tag{16}$$

$$M_j = M_j^{CC} + M_j^{CV} + M_j^{R} + M_j^{T} \tag{17}$$

$$\phi_j = \frac{\varepsilon_{cc}}{C_{b,j}} \tag{18}$$

Lateral forces and lateral displacements can be calculated with the determined moments and curvatures at the corresponding stage of the strain distribution. $F_{L,j}$ is simply determined by Equation 19. However, more calculations are required to determine the lateral displacement from the curvature. ϕ_p is the difference between ϕ_u and ϕ_y, given as Equation 20. The plastic curvature is assumed to be constant over the equivalent plastic hinge length, which is calibrated to give the same plastic rotation as occurs in the real column. From analyses and test results (Priestley *et al.*, 1996), a reasonable estimate for the plastic hinge length when the plastic hinge forms against a supporting member, such as the footing in Figure 6, is given by Equation 21.

$$F_{L,j} = \frac{M_j}{L} \tag{19}$$

$$\phi_p = \phi_u - \phi_y \tag{20}$$

$$L_p = 0{\cdot}8L_H + 0{\cdot}022 f_{ye} d_{bl} \geqslant 0{\cdot}044 f_{ye} d_{bl} \ (f_{ye} \text{ in MPa}) \tag{21}$$

The second term in Equation 21 makes allowance for additional rotation at the critical section resulting from strain penetration of the longitudinal reinforcement into the footing. The plastic rotation is given by Equation 22. Excluding all additional flexibility effects, the yield displacement can be calculated approximately by Equation 23. The plastic displacement (Δ_p) includes the component due to the plastic rotation (θ_p) and additional elastic displacement resulting from the increase in moment from nominal moment capacity (M_n) to maximum moment capacity (M_u). The plastic displacement is given by Equation 24. Using derived equations,

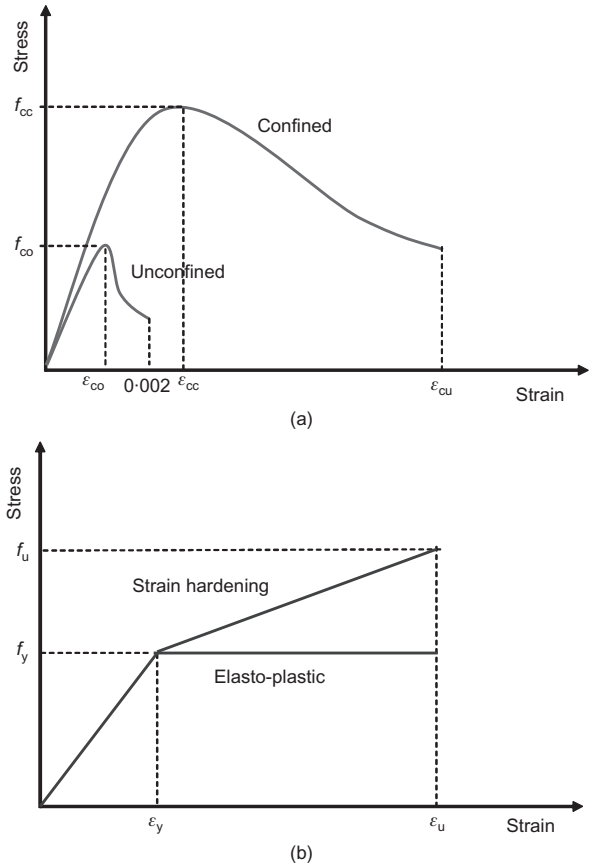

Figure 4. Idealised stress–strain curves: (a) concrete; (b) steel

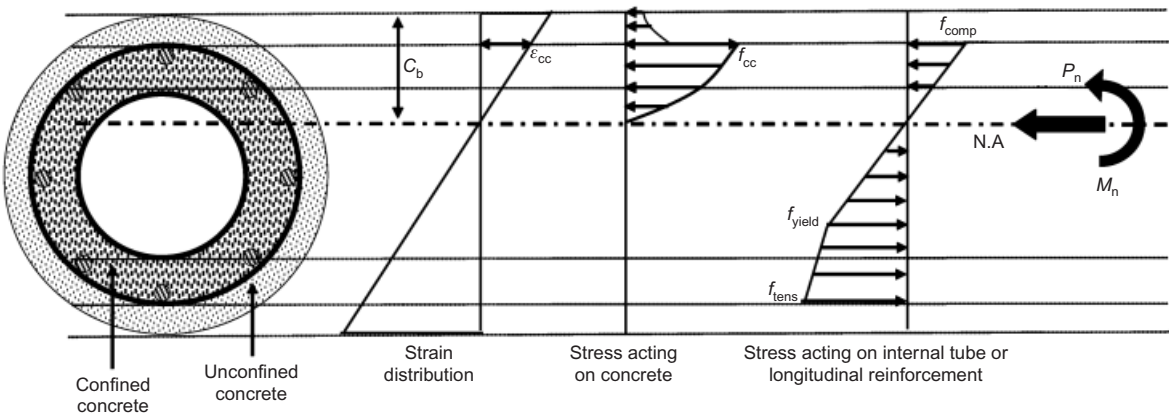

Figure 3. Section analysis using strain compatibility and layer-by-layer approach

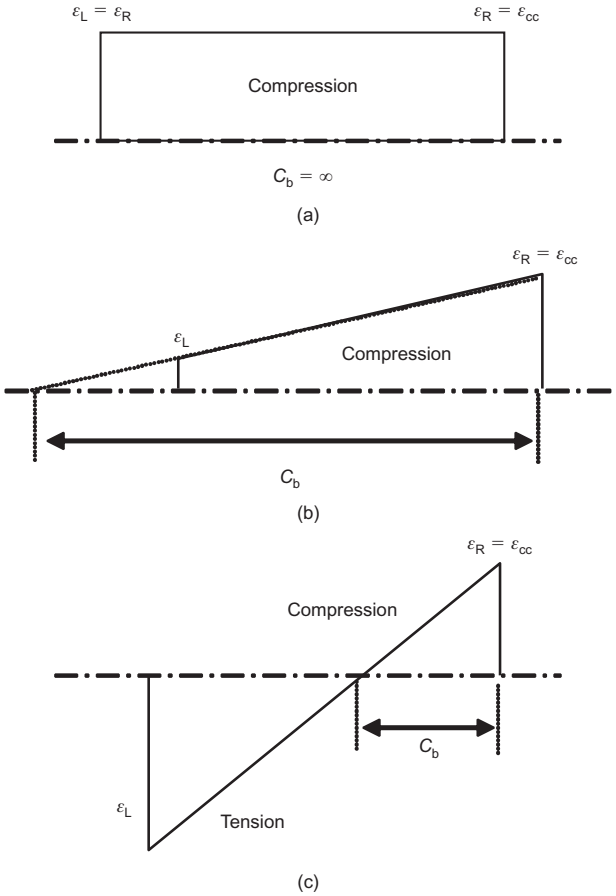

Figure 5. Stages of strain distribution: (a) initial stage; (b) middle stage; (c) final stage

a column analysis program was coded in FORTRAN language.

$$\theta_p = L_p\phi_p = L_p(\phi_u - \phi_y) \tag{22}$$

$$\Delta_y = \frac{\phi_y L_H^2}{3} \tag{23}$$

$$\Delta_p = \left(\frac{M_u}{M_n} - 1\right)\Delta_y + L_p\phi_p(L - 0{\cdot}5L_p) \tag{24}$$

Experiment

Design and construction of specimen

A total of four columns were tested, including three different ICH RC columns and one solid RC column. The three ICH RC columns had different internal tubes. One had a flat steel tube (ICH RC–ST column). Another had a corrugated steel tube (ICH RC–CT column). The last one had a polyvinyl chloride (PVC) tube (ICH RC–PVC column). The main parameters considered in this test were internal confining pressure and failure modes. All columns were designed to have 700 mm of outer diameter, 40 mm thickness of the cover concrete. The height from the top of the footing to the loading point was 2650 mm. The diameter of transverse reinforcement was 13 mm. Its spacing was 66·7 mm and 200 mm for the plastic and elastic region respectively. The ICH RC columns had 406·4 mm of diameter for the hollow section. The diameter of longitudinal reinforcement was 19 mm. To have equal longitudinal reinforcement ratios (1·33%), the ICH RC columns had 12 longitudinal, and the solid RC column had 16 longitudinal. The thicknesses of the flat steel tube, the corrugated steel tube, and PVC tube were 9 mm, 2 mm and 13 mm respectively. The corrugated tube had 68 mm of pitching wave, 13 mm of wave height, and 17·5 mm of wave radius. Figure 7 shows the cross-section of the designed column specimens.

The developed analysis model assumes the concrete and the internal tube are completely bonded. If they are not bonded, a slip will occur between them under flexural loading. The slip prevents a composite structure from exerting its full strength in practice. The complete composition makes it possible to assume the strain distribution is continuous along the bending axis. This assumption makes the analysis simple. For this reason, shear connectors were designed and fabricated on the outer surface of the internal tube as shown in Figure 8. They were arranged with 200 mm of spacing in the plastic region and 400 mm of spacing in the elastic region along the height of the column. The shear

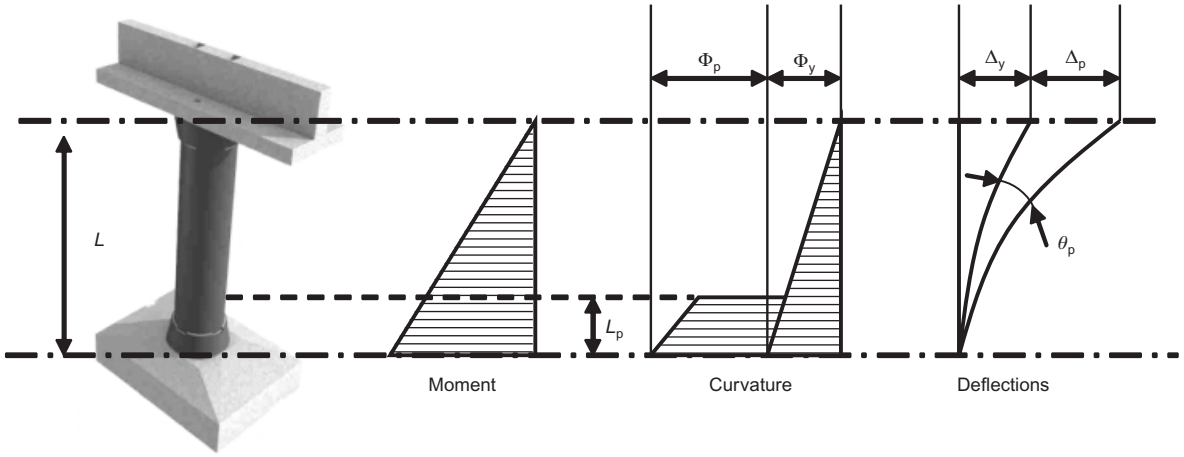

Figure 6. Inelastic deformation of a column

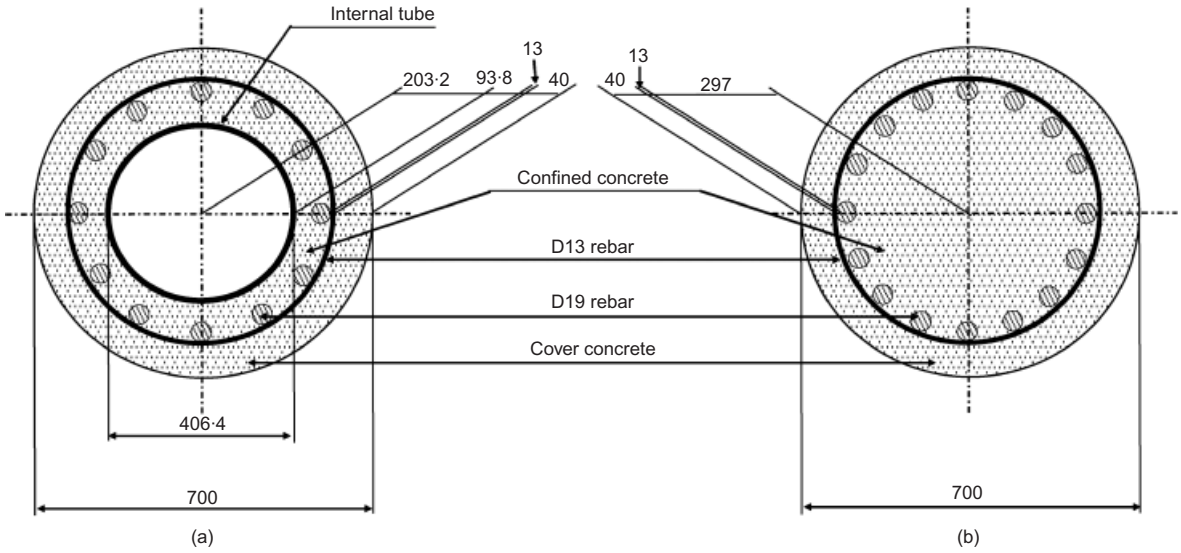

Figure 7. Cross-sectional dimension of designed column (mm): (a) ICH RC column; (b) solid RC column

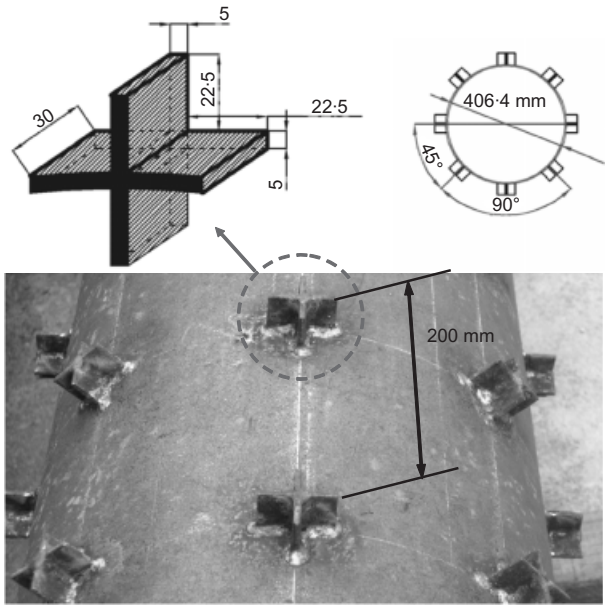

Figure 8. Shear connectors on the steel tube (mm)

connector was designed to have a cross(+)-shaped section to play the roles of a shear connector for the composition and a stiffener to prevent the local buckling of the internal tube. Therefore, its cross-sectional area and height were designed to be equal to those of a general shear connector currently used. The spacing was determined to resist expected shear force in the test based on the analysis result. It could be designed to have enough length as a stiffener to prevent the local buckling of the internal tube. However, a study of its required length as a stiffener has not been completed yet. Therefore, it is not confirmed if this cross-shaped shear connector would prevent the local buckling of the internal tube. The specimens under construction are shown in Figure 9. From the 28-day mould test, the compressive strength of concrete was 21·72 MPa. Table 1 provides summarised material properties. By Equation 6 and Equation 9, the minimal required thicknesses of the internal tubes were calculated as 1·28 mm, 1·53 mm and 12·72 mm for the ICH RC–ST, ICH RC–CT and ICH RC–PVC column specimens respectively. Therefore, all specimens were expected to show failure mode 2.

Experimental programme

Before the test, analyses were performed for the column specimens by using the proposed column model. Predicted axial load against bending moment interaction curves and lateral force against lateral displacement relations were plotted in Figure 10. The ICH RC–ST column specimen was expected to show much higher strength than the solid RC column specimen owing to additional bending strength by the internal steel tube although it had a hollow section. But the ICH RC–CT and ICH RC–PVC column specimens were expected to show lower strengths than the solid RC column because their internal tubes contribute to only the confinement of the concrete. This was because their internal tubes had low strengths with small thickness (ICH RC-CT) and low yield strength (ICH RC–PVC). Figure 10(b) shows the compared lateral force–lateral displacement relations when the confining effect was considered (noted as 'confined') and not considered (noted as 'unconfined'). As shown in Figure 10(b), when the confining effect was considered, the specimens showed higher strengths and larger ductility. Table 2 shows the numerical data of balanced moments and axial strengths of the tested columns.

A quasi-static test with a displacement control was performed. By using a hydraulic actuator with 2 MN capacity, cyclic lateral loads were applied to the specimens as the planned drift ratios shown in Figure 11. The axial load was determined as 10% of the axial strength of each specimen based on the analysis results

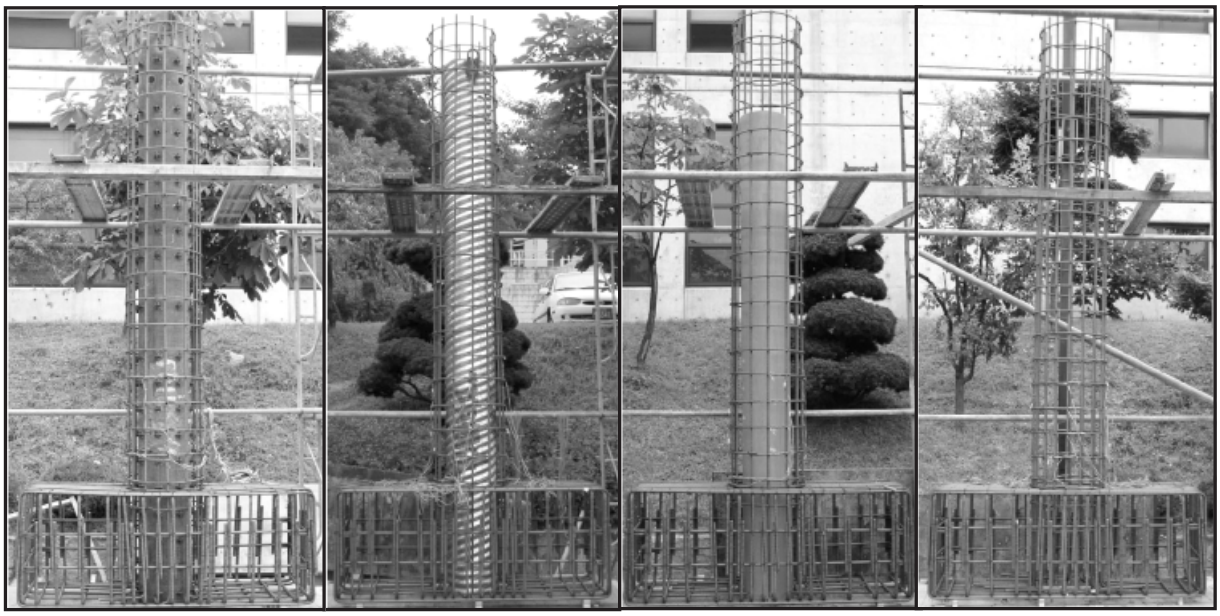

Fig. 9. Column specimens under construction: (a) ICH RC–ST column; (b) ICH RC–CT column; (c) ICH RC–PVC column; (d) solid RC column

Table 1. Material properties (unit = MPa)

Material	Yield strength	Ultimate strength
Longitudinal reinforcement	189·5	288·9
Transverse reinforcement	232·2	300·8
Flat steel tube	378·2	588·6
Corrugated steel tube	206·0	274·1
PVC tube	29·4	49·1

shown in Figure 10(a). The applied axial loads are summarised in Table 3. For the measurement of lateral displacements of the column specimens, three linear variable differential transducers (LVDTs) and two wire gauges were installed. Figure 12 shows the set-up of the specimen and the installed gauges.

Experimental results and discussion

The test was performed until the column specimen lost its stiffness by the failure of the longitudinal reinforcement. Figure 13 shows the fractured column specimens after the test. All the specimens showed 'failure mode 2' as expected. The ICH RC–ST column still resisted with its internal steel tube after first failure of the longitudinal reinforcement. However, the internal steel tube tore quickly and the ICH RC column lost its stiffness immediately by the failure of another longitudinal reinforcement.

The measured lateral load against lateral displacement responses based on the LVDT readings of all the tested column specimens are shown in Figure 14. They are also compared with the analysis results which were plotted in Figure 10(b). They show that the confining effect of concrete must be considered for reasonable analyses. In general, the initial slopes and the maximum loads of the analysis results agreed with the experimental results. In addition, the ultimate displacements from the analysis and experimental results coincided. For the ICH RC–ST column specimen, the analysis results showed about 8% lower peak strength (486·43 kN) than the experimental results (529·92 kN). For the ICH RC–CT, ICH RC–PVC and solid RC column specimens, they showed 9% (250·83 kN), 3% (253·13 kN) and 8% (317·73 kN) higher strengths than the experimental results (229·10 kN, 246·00 kN and 294·83 kN) respectively. They are summarised in Table 4. The ultimate displacements from the experimental result were calculated as the method suggested by Park (1988).

Figure 15 shows the lateral load against lateral displacement envelope curves based on the hysteresis curves in Figure 14. As shown in Figure 14 and Figure 15, the ICH RC column specimen showed much higher strength (529·92 kN) than the solid RC column specimen (317·73 kN). It means an ICH RC–ST column can replace a solid RC column, with a smaller diameter for the equal strength. The bending strength of an ICH RC–ST column can be controlled by the thickness of the internal tube without the enlargement of its diameter. The ICH RC–CT and ICH RC–PVC column specimens showed lower strengths than the solid RC column specimens. Because the corrugated tube was very thin and the PVC tube had very low yield strength, they contributed only to the confining effect, and their contribution to the additional bending strength was minimal.

Based on the hysteresis curves in Figure 14, the

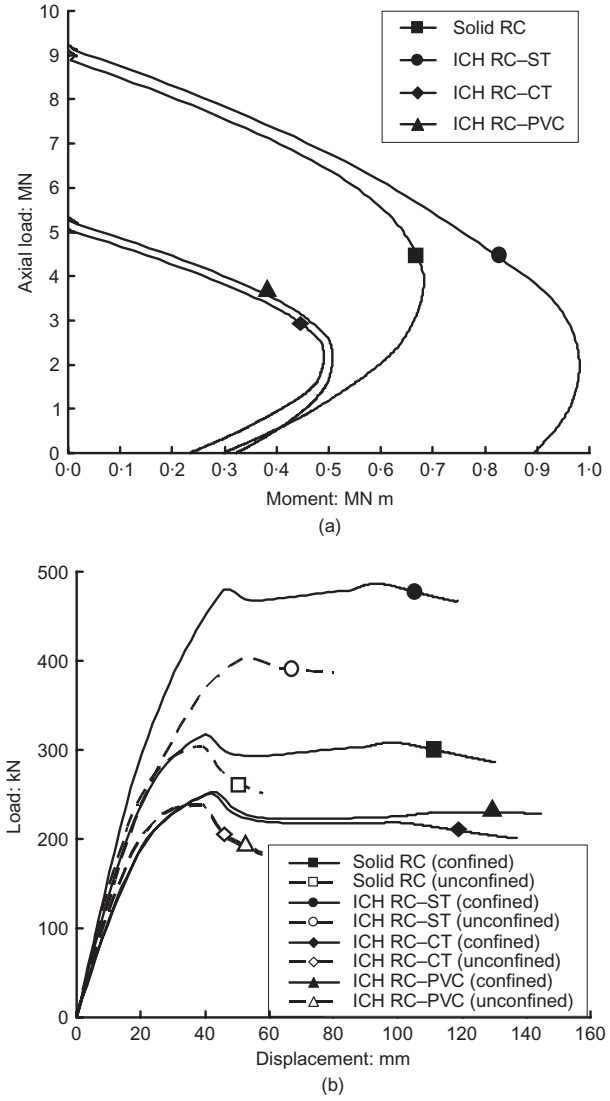

Figure 10. Predicted behaviour of column specimen: (a) axial load–bending moment interaction; (b) lateral force–lateral displacement

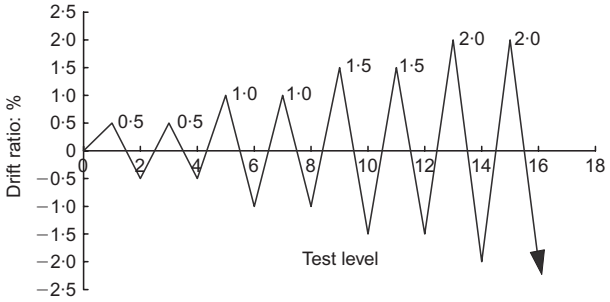

Figure 11. Loading history

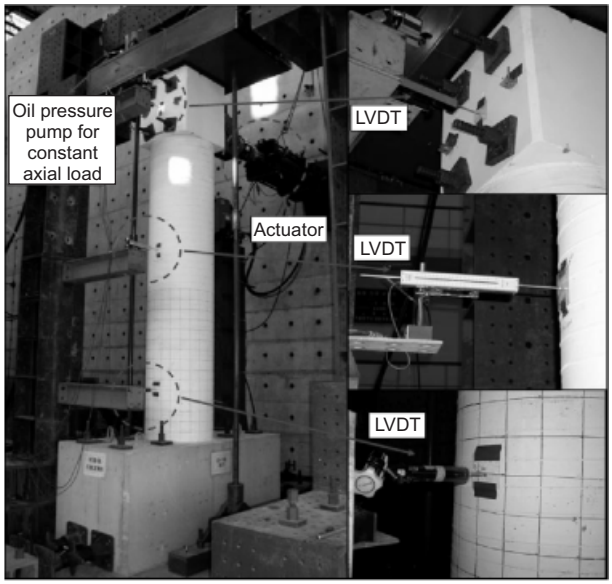

Figure 12. Set-up of column specimen

energy ductility factors were calculated and summarised in Table 5. The yield and ultimate displacements were calculated by the method suggested by Park (1988). Although the ICH RC–ST column specimen has much higher ultimate energy than any other column specimen, it shows a lower energy ductility factor than the ICH RC–CT and solid RC column specimens. This results from much higher yield energy of the ICH RC–ST column than those of other columns. If it has a smaller diameter provided from equal bending strength to the solid RC column specimen, its ductility factor will increase. The ICH RC–CT column specimen shows a satisfactory ductility factor. The type or the thickness of the internal tube can be chosen for the design purpose such as ductility or energy-absorbing capacity of the ICH RC column. Table 6 shows all calculated energy data from the test results and it gives useful information to calculate absorbed energy of the column specimens shown in Figure 16.

Figure 16 shows the energy-absorbing capacities of

Table 2. Balanced axial load and moment

Specimen	P_0: kN	M_0: kN m	P_b: kN	M_b: kN m	e_b: mm
ICH RC–ST	9225·93	895·17	1994·47	980·94	491·83
ICH RC–CT	5063·27	233·67	2179·91	490·81	225·15
ICH RC–PVC	5340·41	322·25	2664·29	507·27	190·40
Solid RC	9104·88	297·47	3917·91	682·46	174·19

Table 3. Applied axial load

Specimen	ICH RC–ST	ICH RC–CT	ICH RC–PVC	Solid RC
Applied axial load: kN	922·6	506·3	534·0	910·5

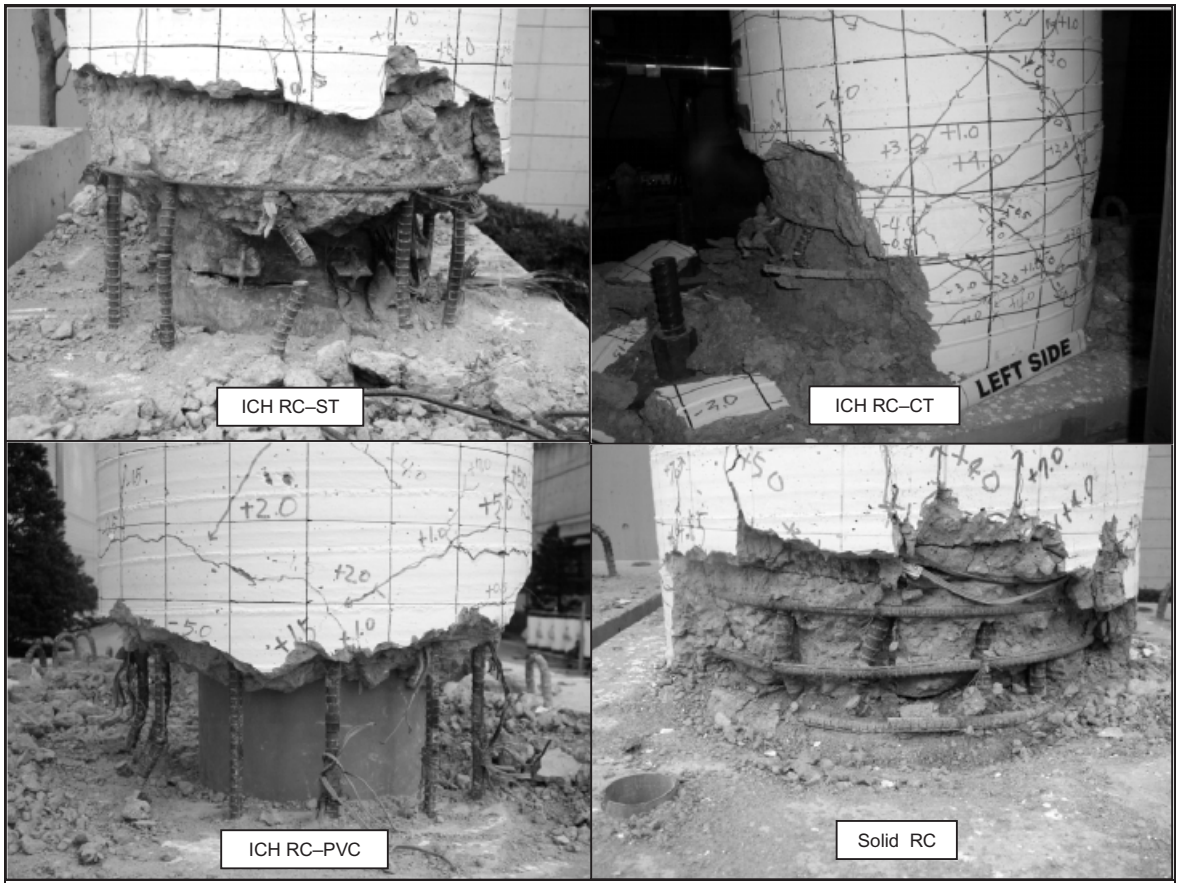

Figure 13. Fractured specimens

the column specimens. The ICH RC–ST column showed almost a double capacity (185%) of the solid RC column in energy absorption. The ICH RC–PVC and ICH RC–CT columns showed similar energy-absorbing capacity to each other. Their plots are overlapped in many parts. This results from the fact that their internal tubes mostly contribute to the confining effect only. Table 7 gives additional information to calculate the damage indices of the column specimens shown in Figure 17 with Table 6.

Figure 17 shows damage indices (DI) of the column specimens calculated by Equation 25 proposed by Park *et al.* (1985). The reduction factor for an RC column is 0·2, based on the research by Fardis (1995). For the ICH RC columns, 0·2 was used as the reduction factor in this study because there is no research result about DI of an ICH RC column. Figure 17 shows that the ICH RC columns are damaged more quickly than the solid RC column. However, the ICH RC–ST and ICH RC–PVC columns showed similar damage indices and slopes with the solid column. As mentioned previously, the ICH RC–ST column showed the double moment-resisting capacity of the general solid RC column. This is because the internal steel tube contributed to increasing the bending stiffness of the ICH RC column. However, in the ICH RC–PVC column, the PVC tube contributes little to the bending stiffness of the column because the PVC tube has a small modulus of elasticity and low yield strength. Therefore, an ICH RC–ST column shows superior moment-resisting capacity to the other columns. However, DI depends mainly on the ratios of d_m to d_u and E_n to Q_y. The ICH RC–ST column and the ICH RC–PVC column have similar ratios to d_m to d_u. This can cause them to have similar DIs. The ICH RC–ST column absorbs much larger energy and has large yield strength too. The ICH RC–PVC column absorbs small energy and has small yield strength. For these reasons, they can have similar DIs.

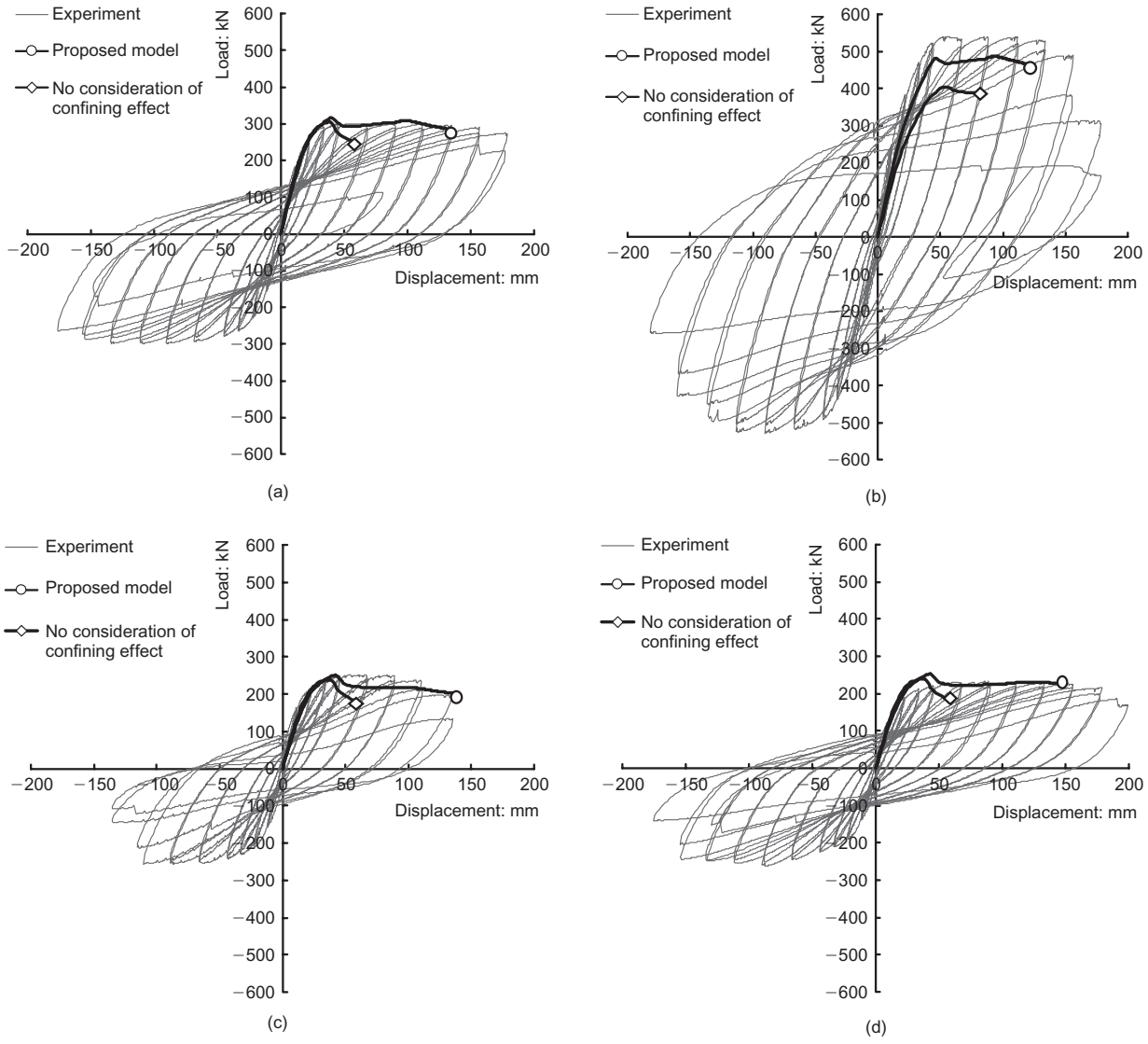

Figure 14. Experimental and analysis results: (a) solid RC column; (b) ICH RC–ST column; (c) ICH RC–CT column; (d) ICH RC–PVC column

Table 4. Maximum load and ultimate strength

Specimen	Maximum load: kN			Ultimate displacement: mm		
	Analysis	Experiment	Ratio: %	Analysis	Experiment	Ratio: %
ICH RC–ST	486·43	529·92	91·79	118·56	156·00	76·00
ICH RC–CT	250·83	229·10	109·48	137·24	129·00	106·39
ICH RC–PVC	253·13	246·00	102·90	144·65	157·00	92·13
Solid RC	317·73	294·83	107·77	130·22	176·78	73·67

The rapid slope of the ICH RC–CT column is supposed to result from the corrugation of its internal tube, and more research for the reduction factor of ICH RC columns is required for a reasonable comparison.

$$DI = \frac{d_m}{d_u} + \frac{\beta}{Q_y d_u} \int dE_n \qquad (25)$$

Conclusion

The behaviour of an ICH RC column was investigated by analyses and experiments. A non-linear ICH RC column model was suggested and column tests were performed. The suggested column model considered the confining effect of concrete. The analysis

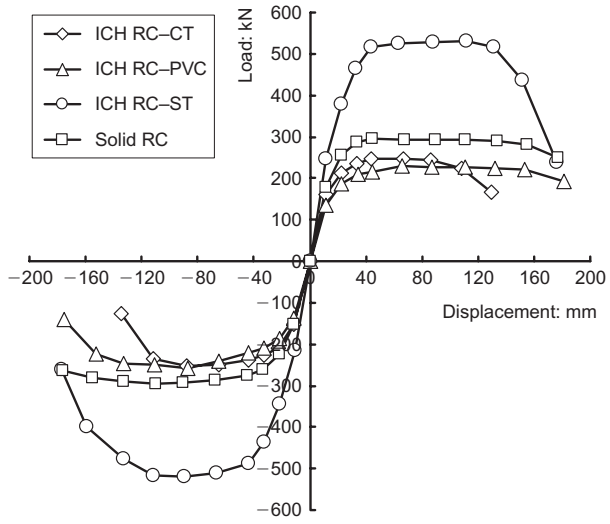

Figure 15. Envelope curves

results showed acceptable agreement with the test results. It shows the suggested model is reasonable and the confining effect of concrete must be considered to predict the behaviour of an ICH RC column. Three different ICH RC columns and one solid RC column were tested. A flat steel tube, a corrugated steel tube and a PVC tube were used as the internal tubes of the ICH RC column specimens. Each type of the ICH RC column showed different behaviour with regard to the type of its internal tube. The stiffness of the internal tube, represented as its thickness, mainly affected the behaviour of the ICH RC column. The ICH RC–ST column specimen showed 200% of bending strength and 150% of energy-absorbing capacity of the solid RC column specimen. Because the strength of the ICH RC column can be controlled by the thickness of its internal tube without any change of its diameter, it is possible to build a high-strength column with a small diameter.

Acknowledgement

This work was supported by the Korea Research Foundation Grant funded by the Korean Government (MOEHRD) KRF-2007-357-D00245.

Table 5. Energy ductility factor

Specimen	ICH RC–ST	ICH RC–CT	ICH RC–PVC	Solid RC
Yield energy: kN m	8·99	3·05	4·47	4·11
Ultimate energy: kN m	70·65	27·93	33·46	47·10
Energy ductility factor	7·86	9·15	7·48	11·45

Table 6. Calculated energy

Calculated energy: kN m	Specimen type	Drift ratio: %									
		0·50	1·00	1·50	2·00	3·00	4·00	5·00	6·00	7·00	8·00
Input energy	Solid RC	4·42	12·58	22·78	32·81	58·76	84·00	110·03	138·09	161·63	155·02
	ICH RC–ST	5·94	17·72	33·06	52·38	106·42	162·66	228·20	280·67	293·44	256·36
	ICH RC–CT	4·48	11·75	19·53	27·60	48·13	69·13	87·15	68·93	—	—
	ICH RC–PVC	3·85	10·04	17·14	24·55	43·73	63·38	83·11	103·44	118·99	104·43
Cumulative input energy	Solid RC	4·42	17·00	39·77	72·59	131·35	215·35	325·38	463·47	625·10	780·12
	ICH RC–ST	5·94	23·66	56·72	109·10	215·52	378·18	606·38	887·05	1180·49	1436·85
	ICH RC-CT	4·48	16·22	35·75	63·35	111·48	180·60	267·75	336·68	—	—
	ICH RC–PVC	3·85	13·90	31·04	55·59	99·32	162·69	245·80	349·24	468·23	572·66
Absorbed energy per cycle	Solid RC	1·56	4·70	11·06	19·00	43·01	67·00	91·89	118·89	142·35	138·35
	ICH RC–ST	1·80	5·39	11·76	23·86	73·60	126·82	190·93	244·67	264·52	238·85
	ICH RC–CT	1·56	4·50	9·49	15·99	34·77	54·08	72·32	59·15	—	—
	ICH RC–PVC	1·36	3·81	8·32	14·11	31·21	49·30	67·82	87·49	102·72	89·71
Cumulative absorbed energy	Solid RC	1·56	6·26	17·32	36·32	79·33	146·32	238·21	357·10	499·45	637·80
	ICH RC–ST	1·80	7·19	18·95	42·81	116·41	243·23	434·17	678·83	943·36	1182·21
	ICH RC–CT	1·56	6·06	15·55	31·54	66·31	120·39	192·71	251·87	—	—
	ICH RC–PVC	1·36	5·18	13·50	27·61	58·82	108·12	175·94	263·42	366·14	455·86
Elastic strain energy	Solid RC	3·69	10·57	18·37	25·41	39·03	52·73	65·00	77·54	87·18	90·86
	ICH RC–ST	5·10	15·83	29·62	43·91	66·99	92·81	116·83	131·03	129·96	88·27
	ICH RC–CT	3·54	9·48	15·43	21·28	32·57	43·21	50·51	38·48	—	—
	ICH RC–PVC	3·07	8·29	13·91	19·46	30·75	42·25	52·65	62·38	68·30	59·65

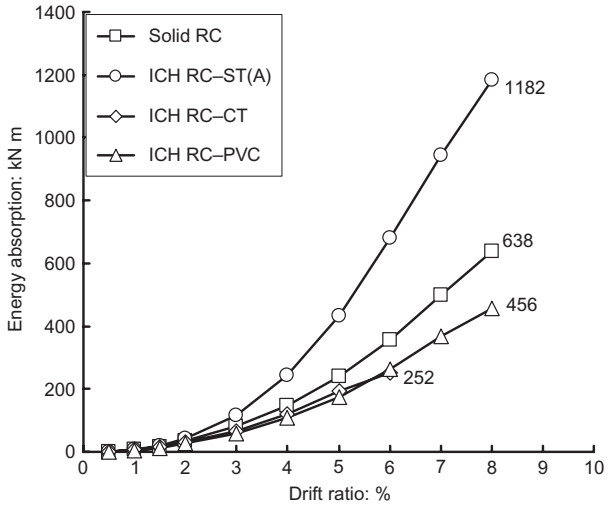

Figure 16. Energy absorption

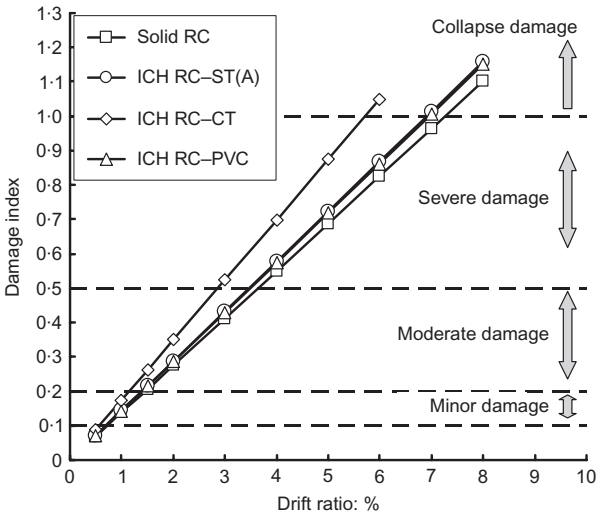

Figure 17. Damage index

Table 7. Displacement and damage index

Drift ratio: %	Maximum displacement per cycle: mm	Damage index			
		Solid RC	ICH RC–ST	ICH RC–CT	ICH RC–PVC
0·50	11·25	0·07	0·07	0·09	0·07
1·00	22·50	0·14	0·14	0·17	0·14
1·50	33·75	0·21	0·22	0·26	0·22
2·00	45·00	0·27	0·29	0·35	0·29
3·00	67·50	0·41	0·43	0·52	0·43
4·00	90·00	0·55	0·58	0·70	0·57
5·00	112·50	0·69	0·72	0·87	0·72
6·00	135·00	0·83	0·87	1·05	0·86
7·00	157·50	0·96	1·01	—	1·01
8·00	180·00	1·10	1·16	—	1·15
Ultimate displacement: mm		164·00	156·00	129·00	157·00

References

Chung HS, Yang KH, Lee YH and Eun HC (2002) Stress–strain curve of laterally confined concrete. *Engineering Structures* **24(9)**: 1153–1163.

Desayi P, Iyengar KTSR and Reddy TS (1978) Equations of stress–strain curve of concrete confined in circular steel spiral. *Matériaux et Constructions*, **11(5)**: 339–345.

Fafitis A and Shah SP (1985) Predictions of ultimate behavior of confined columns subjected to large deformations. *ACI Journal* **82(4)**: 423–433.

Fardis MN (1995) Damage measures and failure criteria for reinforced concrete members. *Proceedings of the 10th European Conference on Earthquake Engineering, Rotterdam*, **2**, 1377–1382.

Han TH, Lim NH, Han SY, Park JS and Kang YJ (2008) Nonlinear concrete model for an internally confined hollow reinforced concrete column. *Magazine of Concrete Research* **60(6)**: 429–440.

Iyengar KTSR, Desayi P and Reddy TS (1970) Stress–strain characteristics of concrete confined in steel binders. *Magazine of Concrete Research* **22(72)**: 173–184.

Kerr AD and Soifer MT (1969) The linearization of the prebuckling state and its effects on the determined instability load. *Journal of Applied Mechanics* **36**, 775–785.

Kilpatrick AE and Ranagan BV (1997) *Deformation-control analysis of composite concrete columns*. School of Civil Engineering, Curtin University of Technology, Perth, Western Australia. Research Report No. 3/97.

Kim YJ, Han TH, Lee SG, Kim DY and Kang YJ (2001) Ductility of circular hollow reinforced concrete piers internally confined by steel tube. *Proceedings of the International Conference on Steel and Composite Structures*, Pusan, South Korea, Techno Press, pp. 1301–1310.

Mander JB, Priestley MJN and Park R (1984) *Seismic design of bridge piers*. University of Canterbury, New Zealand. Research Report No. 84-2.

Park R (1988) Ductility evaluation from laboratory and analytical testing. *Proceedings of the 9th World Conference on Earthquake Engineering, Tokyo*, **8**, 605–616.

Park YJ, Ang AH-S and Wen YK (1985) Seismic damage analysis and damage-limiting design of RC buildings. Civil Engineering Studies Reports SRS 516, University of Illinois, Urbana, IL, 1984.

Popovics S (1973) A numerical approach to the complete stress–strain curves of concrete. *Cement and Concrete Research* **3(5)**: 583–599.

Priestley MJN, Seible F and Calvi GM (1996) *Seismic design and retrofit of bridges*. Wiley, New York.

Roy HEH and Sozen MA (1964) Ductility of concrete. *Proceedings of the International Symposium on the Flexural Mechanics of Reinforced Concrete*, ASCE–ACI Miami, FL, pp. 213–224.

Sakino K and Sun YP (1984) Stress–strain curve of concrete con-

fined by rectilinear hoop. *Journal of Structural and Construction Engineering Transactions of the Architectural Institute of Japan* **461**: 95–104.

Scott BD, Park R and Priestley MJN (1982) Stress–strain behaviour of concrete confined by overlapping hoops at low and high strain rates. *ACI Journal* **79(1)**: 13–27.

Sheikh SA and Uzumeri SM (1980) Strength and ductility of tied concrete columns. *Journal of the Structural Division, ASCE* **106(ST5)**: 1079–1102.

Sheikh SA and Uzumeri SM (1982) Analytical model for concrete confinement in tied columns. *Journal of the Structural Division, ASCE* **108(12)**: 2703–2722.

Timoshenko SP and Woinowsky-Krieger S (1959) *Theory of plates and shells*. McGraw-Hill, Singapore.

Vallenas J, Bertero VV and Popov EP (1977) *Concrete confined by rectangular hoop subjected to axial loads*. Earthquake Engineering Research Center, University of California, Berkeley, Report No. UCB/EERC-77/13, p. 114.

Discussion contributions on this paper should reach the editor by 1 July 2010